Chemical Science

ROYAL SOCIETY OF CHEMISTRY

EDGE ARTICLE

Cite this: *Chem. Sci.*, 2021, **12**, 6588

All publication charges for this article have been paid for by the Royal Society of Chemistry

Exploring Cu/Al cluster growth and reactivity: from embryonic building blocks to intermetalloid, open-shell superatoms†

Max Schütz,[ab] Christian Gemel,[ab] Maximilian Muhr,[ab] Christian Jandl,[b] Samia Kahlal,[c] Jean-Yves Saillard[c] and Roland A. Fischer *[ab]

Received 14th January 2021
Accepted 30th March 2021

DOI: 10.1039/d1sc00268f

rsc.li/chemical-science

Cluster growth reactions in the system $[Cu_5](Mes)_5$ + $[Al_4](Cp^*)_4$ (Mes = mesitylene, Cp* = pentamethylcyclopentadiene) were explored and monitored by *in situ* LIFDI-MS and ^{1}H-NMR. Feedback into experimental design allowed for an informed choice and precise adjustment of reaction conditions and led to isolation of the intermetallic cluster $[Cu_4Al_4](Cp^*)_5(Mes)$ (**1**). Cluster **1** reacts with excess 3-hexyne to yield the triangular cluster $[Cu_2Al](Cp^*)_3$ (**2**). The two embryonic $[Cu_4Al_4](Cp^*)_5(Mes)$ and $[Cu_2Al](Cp^*)_3$ clusters **1** and **2**, respectively, were shown to be intermediates in the formation of an inseparable composite of the closely related clusters $[Cu_7Al_6](Cp^*)_6$ (**3**), $[HCu_7Al_6](Cp^*)_6$ ($\mathbf{3_H}$) and $[Cu_8Al_6](Cp^*)_6$ (**4**), which just differ by one Cu core atom. The radical nature of the open-shell superatomic $[Cu_7Al_6](Cp^*)_6$ cluster **3** is reflected in its reactivity towards addition of one Cu core atom leading to the closed shell superatom $[Cu_8Al_6](Cp^*)_6$ (**4**), and as well by its ability to undergo σ(C–H) and σ(Si–H) activation reactions of $C_6H_5CH_3$ (toluene) and $(TMS)_3SiH$ (TMS = tris(trimethylsilyl)).

Introduction

Metal clusters are fascinating chemical objects. Their targeted generation in the gas-phase or in solution as unligated as well as ligand stabilized species has been a "hot topic" of interdisciplinary research for a long time. The famous Schmid cluster $[Au_{55}](PPh_3)_{12}Cl_6$, discovered in 1981,[3] and the mystery of its true composition and structure may serve as an illuminating example.[4]

Clusters mark the transition from the molecular to the bulk state of matter. The increased understanding of their structural, electronic and physical properties, as well as the development of novel techniques for their synthesis, separation and characterization opened new avenues for cluster chemistry. Advances in computational theoretical analysis revealed interesting connections between electronic structure and reactivity patterns. Examples include small molecule activation (CO, CO_2, H_2, H_2O, *etc.*) at 3d transition metal 13-atom clusters[5] and the reactivity of NO and O_2 at Al doped Cu cluster cations.[6]

Metallic elements dominate the periodic table. Considering the combinatorial space of mixed-metal clusters $[M_a^1M_b^2M_c^3\ldots]$- the enormous and largely unexplored playground becomes obvious since every atom counts in metal cluster chemistry and physics. Likewise, solid-state alloys and intermetallic phases provide rich opportunities for exciting discoveries. They are useful, in particular, as novel materials in heterogeneous catalysis.[7]

In cluster research, structure–reactivity relationships have mostly been reported for gas-phase clusters or gas-phase generated clusters deposited on a support.[8–11] By sputtering or laser ablation of metallic targets under high-vacuum, a rich set of (bimetallic) gas-phase metal clusters is accessible.[12,13] Noteworthy, mass-spectrometry is thereby a key tool for the assessment of cluster identities and of reaction products.[14–16]

We have been attracted to metal clusters as a research objective from the perspective of challenges in organometallic synthesis across the periodic table,[17–19] and we are much inspired by linking solid state chemistry of intermetallics with the molecular chemistry of mixed metal clusters.[20] There are two categories of wet chemical synthetic strategies for obtaining ligand protected *intermetalloid* clusters $[M_n](R)_m$ ($n \gg m$; M = two or more different metal atoms; n = number of metal atoms aggregated in the cluster core; R = hydrocarbon ligand; square brackets denote the cluster core; round brackets denote the core protecting heteroatom-free, all-hydrocarbon ligand shell). Of note, the described nomenclature chosen in this manuscript is different from the IUPAC recommendations for transition metal compounds. However, the authors consider the presented way

[a]*Department of Chemistry, Technical University Munich, Lichtenbergstrasse 4, D-85748 Garching, Germany. E-mail: roland.fischer@tum.de*

[b]*Catalysis Research Centre, Technical University Munich, Ernst-Otto-Fischer Strasse 1, D-85748 Garching, Germany*

[c]*Univ Rennes, CNRS, ISCR-UMR 6226, F-35000 Rennes, France*

† Electronic supplementary information (ESI) available. CCDC 2054079–2054082. For ESI and crystallographic data in CIF or other electronic format see DOI: 10.1039/d1sc00268f

of formula writing as more intriguing in terms of metal core compositions and valence electron count.

In the "top down" approach, pre-formed ionic cluster subunits are extruded from solid state phases as the parent material by wet-chemical methods with manifold options of cluster core functionalization afterwards. However, control of cluster nuclearity (size) M_n and shape remains very difficult, especially when it comes to bimetallic clusters to be selectively extruded.[20–22] Nevertheless, an extremely rich solution chemistry of *Zintl* clusters has emerged over the past decades.[23,24] Many of these clusters were obtained by the reaction of soluble *Zintl* anions with organic or organometallic precursors.[23]

The alternative "bottom-up" approach relies on molecular organometallic compounds "M^1R^1" and "M^2R^2" (R^1, R^2 refer to specifically suited all-hydrocarbon ligands; the M/R stoichiometry is not specified here) and the intrinsic reactivity of these precursors against each other (Scheme 1). Modulation of the reaction by the choices of solvent, additives (*e.g.* H_2) and by setting of the extrinsic conditions (temperature, pressure) provides deprotection of the metals from their ligand environments and triggers agglomeration of the released atoms M^1 and M^2. Eventually, ligated intermetalloid clusters of the general formula $[M^1_aM^2_b](R^1)_c(R^2)_d$ ($n = a + b$; $m = c + d$; $n \gg m$) are formed and can be spectroscopically characterized in solution and may even be isolated in pure and single crystalline form. The discovery of the M_{55} magic number open-shell superatom cluster $[Cu_{43}Al_{12}](Cp^*)_{12}$ of Mackay structure-type may be regarded as a prove of concept. It is a break-through of our work, continued over two decades,[17–20] on Hume-Rothery intermetallics inspired metal clusters. The cluster was obtained in toluene solution from the reaction of $[Cu]_5(Mes)_5$ with $[Al]_4(Cp^*)_4$ (abbreviated thereafter as "CuMes" and "AlCp*"; Mes = mesityl = 1,3,5-trimethylbenzene-2-yl; $Cp^* = C_5(CH_3)_5$ = pentamethyl-cyclopentadienyl).[2] Fig. 1 illustrates the 2-dimensional landscape of ligated binary clusters with Cu/Al as the example. Our research described in this article targets the area in between the *n*(Al) and *n*(Cu) axes.

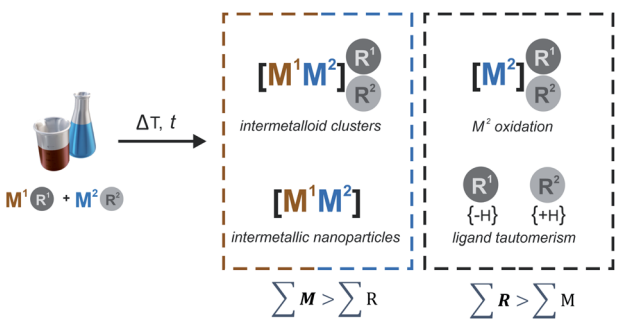

Scheme 1 General concept for the bottom-up synthesis of ligated intermetalloid clusters $[M_n](R)_m$ ($n \gg m$; M = two or more different metal atoms, *e.g.* M^1, M^2; *n* = number of metal atoms aggregated in the cluster core; R = hydrocarbon ligand, *e.g.* R^1, R^2; square brackets denote the cluster core; round brackets denote the core protecting ligand shell). Scheme 1 aims to conceptually catch a diversity of elementary reactions of the organometallic precursors M^1R^1 and M^2R^2 during cluster formation. Note that the option $M^1 = M^2$ is possible. More details and examples are described in the text.

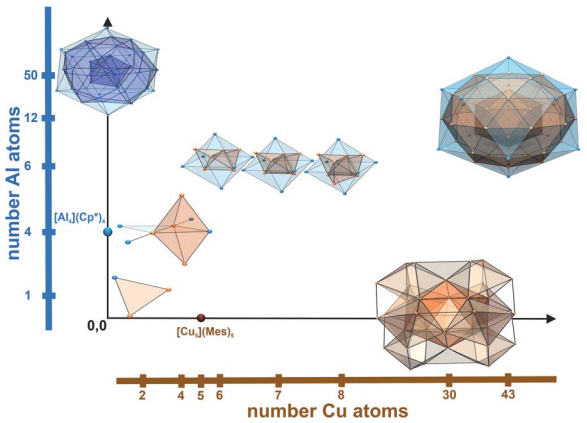

Fig. 1 The two-dimensional landscape of Cu/Al clusters. Only cluster cores are shown for simplicity. The two coordinates *n*(Cu) and *n*(Al) localize the so far experimentally characterized heterometallic species, $[Cu_4Al_4](Cp^*)_5Mes$ (**1**), $[Cu_2Al](Cp^*)_3$ (**2**), $[Cu_7Al_6](Cp^*)_6$ (**3**) and $[Cu_8Al_6](Cp^*)_6$ (**4**) described in this work and $[H_4Cu_6Al_6](Cp^*)_6$ and $[Cu_{43}Al_{12}](Cp^*)_{12}$ from our previous reports.[1,2] The diagram also shows examples of important homometallic clusters such as $[Al_4](Cp^*)_4$, $[Al_{50}](Cp^*)_{12}$ (ref. 25), $[Cu_5](Mes)_5$ and $[Cu_{30}H_{18}](S_2P(OnPr)_2)_{12}$.[26] The hydrocarbon ligand shells are omitted for clarity (color code: Cu = orange-brown; Al = blue).

The organometallic cluster synthesis according to Scheme 1, for example targeting specific points in the Cu/Al landscape of Fig. 1, suffers from numerous obstacles and limitations. Usually, a broad product distribution is observed, often with a subtle dependency on small changes in the selection of precursors and reaction conditions. The delicate interplay of multiple elementary reaction steps, reversible and irreversible in nature have to be considered, often of unknown mechanistic details and kinetic parameters.

Despite the accumulated knowledge of organometallic reaction pathways is quite substantial, the outcome of a bottom-up synthesis of ligated intermetallic clusters is typically unpredictable. The successful isolation of chemically pure clusters often follows a trial-and-error approach, unless being based on profound chemical knowledge and intuition.

Rational reaction concepts guiding the choice of organometallic precursors and conditions include ligand exchange and transmetallation, oxidative addition and reductive elimination, homolytic metal ligand bond cleavage, H-abstraction and H-transfer also involving C–H activation and hydrogenolysis of metal ligand bonds. In the specific case of our Hume-Rothery intermetallics inspired organometallic cluster chemistry,[17–20] the selected transition metal compounds M^1R^1, *e.g.* CuMes, are treated with low valent group 12 and group 13 compounds M^2R^2 such as $([Zn_2]Cp^*)_2$ or AlCp* of Zn(I) and Al(I) oxidation states. Here, the M^2R^2 component exhibits a unique triple function. It acts as reducing agent for M^1R^1 and as a sink or reservoir for R^1 ligands by formation of oxidized M^2 species, *e.g.* MesZnCp* or Mes_2AlCp^*, *i.e.* the formation of $M^2R^1_2$ or $M^2R^1_3$ (and the R^1/R^2 exchanges derivatives). Secondly, the M^2R^2 component can also release M^2 by R^2 transfer and cleavage processes to form alloyed M^1/M^2 cluster cores. The third

function of M^2R^2 is as capping ligand for trapping $[M^1_aM^2_b]$ cores. Our preference of choosing Cp* for R^2 is connected with its haptotropic binding mode and flexibility of adopting to different electronic and steric requirements at the M centers. In addition, Cp* contributes to the stabilization of the cluster species by weak interactions (dispersion forces).

The metal precursors M^1R^1 and M^2R^2 are typically highly reactive and chemically labile. Thus, homolytic metal–ligand bond cleavage or hydrogenolysis may occur and irreversibly lead to (inter-)metallic nanoparticles (NPs) and organic by-products including tautomers $R^{1,2}(-H)$, $R^{1,2}(+H)$ and dimers R^1_2, R^2_2, R^1R^2. Scheme 1 aims to conceptually catch this diversity of elementary reactions. The general synthetic concept illustrated in Scheme 1 is of course oversimplified; it yet illustrates fundamental concepts in wet-chemical, bimetallic cluster chemistry. The synthesis of Pd/Ga, Pd/Al, Pd/In, as well as of Cu/Al and Cu/Zn clusters and coordination compounds can be seen as representative examples thereof.[1,2,27–32] Noteworthy, Scheme 1 is also applicable for many monometallic cluster species if the possibility of $M^1 = M^2$ is taken into account. For example, a plethora of ligated Al clusters is accessible by controlled disproportionation of Al(I)-halide solutions.[33] The details of the involved complex reaction networks are different for each given combination of chosen organometallic precursors and conditions. Precise adjustment of all parameters is crucial for a successful and reproducible synthesis of a certain cluster. However, a rational for setting the parameters to obtain a defined cluster and targeting a specific point in the Cu/Al cluster landscape of Fig. 1 is still not there.

Following the synthetic concept of Scheme 1 and based on our results on the coordination chemistry of low valent group 12 and group 13 species M^2R^2 at transition metal M^1 centers we already were able to obtain a range of so-called "nano brass" Cu/Zn clusters of small and medium nuclearities by combining *Carmona*'s $[Zn_2](Cp^*)_2$ with a variety of Cu(I) complexes as Cu sources. We discovered the embryonic (smallest) building block, the σ-aromatic $[CuZn_2](Cp^*)_3$,[34] and also larger clusters like $\{[Cu_2Zn_5](Cp^*)_5\}^+$ (as $[BAr^F]$-salt) or $[Cu_3Zn_4](Cp^*)_5$.[30] The isolation of defined Cu/Zn cluster species, especially of larger nuclearities, is a sophisticated task. We are facing low yields, complicated product separation and purification procedures and the information about the nature of species formed in a reaction is often based almost solely on the luck of obtaining single crystals suitable for X-ray diffraction. The very same is true for the related Cu/Al cluster "nano bronze" chemistry. So far, we were able to isolate only two examples, the hydrido M_{12} cluster $[H_4Cu_6Al_6](Cp^*)_6$ and the M_{55} cluster $[Cu_{43}Al_{12}](Cp^*)_{12}$ mentioned above.[1,2] Unfortunately, only small amounts of this latter cluster were obtained by selecting single crystals from the raw product. Intermediates, which certainly exist on the way to this M_{55} cluster, could neither be isolated nor unambiguously characterized by *in situ* NMR. However, from the somewhat richer family of isolated and structurally characterized Cu/Zn clusters obtained by a similar chemistry we deduced that there must be an experimental way to shine more light into the dark reaction solutions of the CuMes/AlCp* system.

High resolution mass spectrometry is a powerful method in cluster chemistry and very suitable to establish exact compositions. It is particular versatile for *in situ* analysis of reaction solutions, which has also been demonstrated to be a suitable method for the analysis of carbonyl cluster mixtures in solution.[35–39] However, mass spectrometry has not been widely applied to organometallic cluster chemistry as a tool for monitoring cluster growth, interconversion and the reactivity of clusters towards small molecules. Sample transfer under strict exclusion of air and moisture is needed to avoid decomposition and unwanted parasitic reactions. Also, highly efficient vaporization and smooth ionization techniques are required to yield meaningful and reliable data. Only recently we were able to establish "liquid injection field desorption ionization (LIFDI)" orbitrap mass spectrometry directly coupled to an inert-gas (Ar) reaction chamber (glove box). This instrumentation allowed us to precisely assess the composition of clusters and mixtures of clusters, also directly from the reaction solutions, by detection and analysis of their molecular ion signals and fragmentation patterns.[40]

With this new coupling of synthesis and analysis we were able to identify and isolate a number of new Cu/Al clusters being accessible from CuMes and AlCp*, quite as we expected. The "embryonic clusters" $[Cu_4Al_4](Cp^*)_5Mes$ (**1**) and $[Cu_2Al](Cp^*)_3$ (**2**) were isolated and fully characterized including a detailed bonding analysis on the DFT level of theory. Systematic investigation of cluster growth reactions involving these two building blocks and taking advantage of the direct feedback loop of mass spectrometry of reaction solutions into the parameter optimization of the cluster growth experiment led us to the discovery of the M_{13}/M_{14} cluster mixture $[Cu_7Al_6](Cp^*)_6$ (**3**) $[HCu_7Al_6](Cp^*)_6$ ($\mathbf{3_H}$) and $[Cu_8Al_6](Cp^*)_6$ (**4**) (see Fig. 1). Although these three clusters could not be separated from each other, but are accessible as mixtures only, our mass spectrometric approach allows for detailed insight into their reactivity, *e.g.* C–H and Si–H activation, as a function of the electronic structure (open *vs.* closed shell).

In this article we wish to introduce the reader to this kind of organometallic cluster chemistry and to our research strategy which aims to systematically harvest fundamental insight from the highly complex, combinatorial chemical space addressed by Scheme 1 and Fig. 1. The article is organized in the following way: First, the principles of organometallic Cu/Al cluster synthesis are described, as discussed in this introduction. Second, we present the analytic characterization and providing evidence of the identity of the newly discovered Cu/Al clusters **1–4** in comparison to the already known ones and in relation to Cu/Al intermetallic solid-state phases. Third, the electronic structure of the clusters, *i.e.* bonding analysis on the DFT level of theory, is discussed which leads to the fourth, final chapter dealing with the consequences for chemical reactivity. We found that "open shells open doors". Among the three closely related M_{13}/M_{14} clusters only the radical species $[Cu_7Al_6](Cp^*)_6$ (**3**) undergoes facile C–H and Si–H activation reactions with toluene and $(TMS)_3SiH$ (TMS = $SiMe_3$). Altogether and based on our new examples presented in this article, we claim a uniquely rich intermetalloid chemistry to be explored.

Results

Principles of cluster growth

Formation mechanism of $[Cu_4Al_4](Cp^*)_5(Mes)$ (1). Heating a solution of CuMes with 1.32 eq. of AlCp* in toluene to 75 °C leads to a deep green solution within a few minutes. The reaction progress as monitored by *in situ* ^{1}H-NMR spectroscopy (see ESI, Fig. S1†) indicates rapid formation $[Cu_4Al_4](Cp^*)_5(Mes)$ (**1**) as the major reaction product with three Cp* signals (integral ratio 2 : 2 : 1) as well as one metal coordinated mesityl unit. Also the side products $AlMes_3$ (ref. 41) and Mes_2AlCp^* can be identified in these *in situ* ^{1}H-NMR spectra. Time dependent ^{1}H-NMR spectra indicate the concentration of **1** to be the highest after about 30–80 minutes. As shown in Fig. S1,† only small signals of other Cp* containing species are present at that time, which become more prominent at increased reaction times.

Observation of Mes_2AlCp^* and $AlMes_3$ as side products in the formation of **1** is indicative of partial reduction of Cu(I) to Cu(0) by AlCp* accompanied by ligand transfer reactions between Al and Cu. Notably, 1.5 eq. of $AlMes_3$ and Mes_2AlCp^* are formed per molecule of the $[Cu_4Al_4](Cp^*)_5(Mes)$ cluster **1** according to *in situ* ^{1}H-NMR (see ESI, Fig. S1†). A clear stoichiometric reaction would only include formation of one equivalent $AlMes_3$ (Scheme 2), however, we suppose that the thermal instability of **1** (*vide infra*) leads to a competition between its formation (including formation of $AlMes_3$) and its decay (including formation of Mes_2AlCp^*). **1** can be interpreted as an aggregate of redox-intermediates occurring in the reduction of Cu(I) and its subsequent coordination by AlCp*. We assume similar mechanisms to occur in the early stages of the synthesis of $[Cu_{43}Al_{12}](Cp^*)_{12}$, as Mes_2AlCp^* was also identified as a side product this reaction.[2]

Monitoring the reaction by LIFDI-MS analysis (see ESI, Fig. S15†) reveals a variety of intermetallic Cu/Al clusters with the exact composition being dependent on the reaction time (*vide infra*). However, the molecular ion peak of **1** cannot be detected at all, obviously **1** cannot be ionized without destruction by the LIFDI technique. Also, LIFDI-MS analysis of the isolated single crystals of **1** did not yield a detectable molecular ion signal.

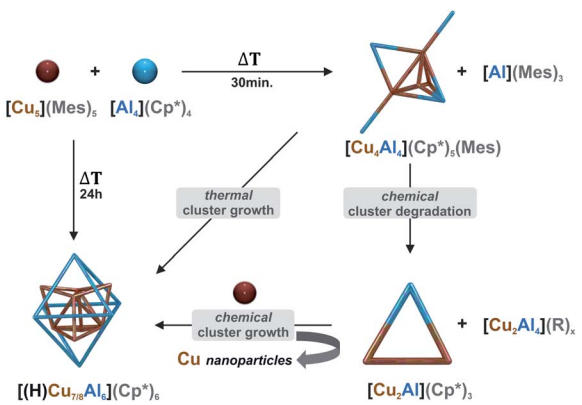

Scheme 2 Synthetic pathways to the new Cu/Al clusters $[Cu_4Al_4](Cp^*)_5(Mes)$ (**1**), $[Cu_2Al](Cp^*)_3$ (**2**), and the inseparable mixture of $[HCu_7Al_6](Cp^*)_6$ ($\mathbf{3_H}$), $[Cu_7Al_6](Cp^*)_6$ (**3**), $[Cu_8Al_6](Cp^*)_6$ (**4**). Cu atoms are illustrated in orange, Al atoms in blue, respectively. For simplicity, only cluster cores are shown. All details of the experimental procedures and analytical characterization data are provided in the ESI.† Upon heating, cluster **1** can be transformed into a mixture of **3**, $\mathbf{3_H}$ and **4**. This mixture can be selectively obtained by a sequence of cluster degradation and growth reactions with additives involving the trimetallic cluster intermediate **2**.

Targeted cluster degradation from $[Cu_4Al_4](Cp^*)_5(Mes)$ 1 to $[Cu_2Al](Cp^*)_3$ (2). The observation of the triangular $[Cu_2Al](Cp^*)_3$ in thermal degradation of isolated **1** (*vide infra*) prompted us to search for a clean synthetic access to this small ("embryonic") building unit of Cu/Al clusters. As alkynes are known to stabilize Cu(I) centers and small Cu clusters,[42,43] we chose 3-hexyne from the organometallic "tool-box" as a degradation agent for **1** to access smaller cluster units. Notably, alkynes are known to react with organometallic Al compounds to yield cycloaddition products.[44]

When a toluene solution of **1** is treated with an excess of 3-hexyne (20 °C), a color change from deep-green to orange-brown is observed within a few minutes. The cluster degradation reaction from **1** to **2** is accompanied by consumption of four equivalents 3-hexyne per molecule of **1** as identified by *in situ* ^{1}H-NMR spectroscopy (see ESI, Fig. S2†). After a total reaction time of four days at room-temperature, **2** is clearly identified as main product by ^{1}H-NMR beside a variety of hexyne- and mesitylene containing side-products. LIFDI-MS analysis of the reaction solution reveals $[Cu_2Al_4](Cp^*)_3(Mes)(Hex)_2$ (Hex = hexyne = C_6H_{10}) to be the main side product of the reaction (see Fig. S16 and Table S2, ESI†).

The presence of $[Cu_2Al_4](Cp^*)_3(Mes)(Hex)_2$ as main side product in the synthesis of **2** (*vide supra*) points towards a cluster degradation mechanism in which 3-hexyne extrudes CuCp* moieties from **1** by stabilizing the electron-deficient, low valent Cu(0) centers through coordination. A detailed analysis of the LIFDI-MS spectra of the reaction reveals a variety of other side products formed (see Table S2, ESI†). Insight into the Cu and Al fate during the reaction can be gained by grouping the reaction products according to their Cu : Al ratio.

Whereas Cu gets mainly incorporated into **2** and some Cu-rich clusters (*e.g.* **3**/**4** among others), the Al stoichiometry of the reaction is balanced by formation $[Cu_2Al_4](Cp^*)_3(Mes)(Hex)_2$ and several other Al-rich clusters and Al-containing coordination compounds. With the two small building blocks **1** and **2** in hand, we set out to explore cluster growth reactions by a detailed study of reaction parameters (see Table S1, ESI†). Obviously, a dynamic composite of three clusters, namely $[Cu_7Al_6](Cp^*)_6$ (**3**), $[Cu_8Al_6](Cp^*)_6$ (**4**) and $[HCu_7Al_6](Cp^*)_6$ ($\mathbf{3_H}$) is available. Analysis of reaction products was therein mainly conducted using LIFDI-MS analysis. Thereby, the assignment of sum formulas to the peaks was verified by comparison between calculated and experimental isotopic patterns, as exemplary shown in Fig. 3a, b for **4** and **2**, in Fig. S21† for $\mathbf{3_H}$, $\mathbf{3_D}$ and **3**. Subtle differences of only one H atom, *e.g.* in **3** and its hydride containing counterpart $\mathbf{3_H}$ are well recognized by a shift of 1 *m*/*z* in the mass spectra (Fig. $3c_1/c_2$).

Thermal treatment of the $[Cu_4Al_4](Cp^*)_5(Mes)$ cluster 1 to yield the $[(H)Cu_{7/8}Al_6](Cp^*)_6$ clusters 3, $\mathbf{3_H}$ and 4. When a solution of $[Cu_4Al_4](Cp^*)_5(Mes)$ is heated to 75 °C, *in situ* ^{1}H-NMR and LIFDI-MS analysis reveal initial formation of

$[Cu_2Al](Cp^*)_3$ (**2**), as well as of Mes_2AlCp^* (see ESI, Fig. S3 and S19†). Further heating leads to consumption of **2** and rather selective formation of **3**, $\mathbf{3_H}$ and **4** as indicated by *in situ* mass spectrometry (Fig. S17†). Obviously, the triangular cluster **2**, which can be considered as smallest building block of Cu/Al clusters is indeed an intermediate in cluster growth reactions from **1** to **3**/**4**. Interestingly, fulvene ($C_{10}H_{14} = (R^2)_2 - 2H$) is observed by *in situ* ^{1}H-NMR spectroscopy, pointing towards an intermolecular C–H bond activation of Cp* as the hydride source for $[HCu_7Al_6](Cp^*)_6$ ($\mathbf{3_H}$). When *in situ* generated solutions of **1** are subjected to thermal treatment at 75 °C in contrast of using pure **1**, different results are obtained (see ESI, Fig. S1 and S15†). Interestingly, ^{1}H-NMR and LIFDI-MS analysis reveal neither formation of **2** nor fulvene, but a much broader variety of Cu/Al clusters after prolonged heating times. Obviously, the presence of $AlMes_3$, which otherwise is removed during the workup of **1**, influences the course of the reaction, most reasonably by promoting ligand exchange reactions, *i.e.* by serving as a "ligand reservoir".

The $[Cu_2Al](Cp^*)_3$ triangular cluster 2 as a building block. In contrast to the labile $[Cu_4Al_4](Cp^*)_5(Mes)$ cluster **1**, the $[Cu_2Al](Cp^*)_3$ triangle **2** is rather temperature-stable and can be heated up to 80 °C in toluene for several hours. The $[Cu_8Al_6](Cp^*)_6$ cluster **4** is formed in trace amounts only, as indicated by ^{1}H-NMR as well as mass spectrometry. The mesityl protected Cu(I) source CuMes acts as a useful reagent for cluster growth. When **2** is treated with 1.2 equivalents of CuMes at elevated temperature (75 °C), formation of Mes_2AlCp^* and $AlMes_3$ is observed in *in situ* ^{1}H-NMR experiments together with HCp*, pentamethylfulvene and decamethyl-1,1′-dihydrofulvalene (see Fig. S4†) as well as some remaining **2**. Obviously, the addition of CuMes to **2** leads to "abstraction" of AlCp*, reduction of Cu(I) units to Cu(0) and oxidation of Al(I) to Al(III) to yield Mes_2AlCp^* as byproduct, thus increasing the amount of Cu(0) and decreasing at the same time the amount of stabilizing AlCp* in the system. Oxidation of some of the Cp* ligands also seems to play a role in Cu(I) reduction. The $[Cu_2Al](Cp^*)_3$ species **2** acts as donator of the Mes deprotection agent for CuMes and as a source of AlCp* as capping agent during the induced $[Cu_n]$ core growth. Consequently, addition of two or more equivalents of CuMes results in rapid formation of a metallic precipitate upon heating, since all available AlCp* in the system is then consumed. LIFDI-MS of the reaction with exactly 1.20 eq. of CuMes with respect to $[Cu_2Al](Cp^*)_3$ (**2**) shows $[Cu_8Al_6](Cp^*)_6$ (**4**) as the only present species beside some unreacted **2** (see Fig. S20†). This result was confirmed by SC-XRD analysis of single crystals showing a pure $[Cu_8]$ core of the cluster without ill-occupied vertices (see Table S4† for crystallographic information). The fate of the stoichiometrically missing Cu in this reaction (see Scheme 2), can be elucidated by TEM analysis on evaporated reaction solutions revealing the presence of larger Cu nanoparticles (5 nm) (see Fig. S34†). However, obtaining a reliable mass or molar balance *n*(Cu) and *n*(Al) is difficult because of the low quantities of materials used. A balanced equation for the reaction can thus not be presented, so far. Noteworthy, **1** is not amongst the reaction products in the investigated cluster growth reactions starting from **2**. We reason that **2** is thermodynamically more stable than **1**, as it is also formed as product in the thermal treatment of **1**. However, the back-reaction of **2** towards **1** might well be feasible by a proper chemical reaction partner.

In conclusion, **2** is therefore clearly an embryonic building block for the formation of larger clusters. Due to its inherent Cu : Al stoichiometry, exact tuning of the amount of Cu(I) added is necessary for the generation of larger Cu/Al clusters.

Alternative access to the cluster composite $\mathbf{3_H}$/4. An alternative access to the cluster composite $\mathbf{3_H}$/**4** was identified by reacting the trinuclear copper hydride precursor $[H_3Cu_3](dppz)_3$ with AlCp* (dppbz = 1,2-bis(diphenylphosphino)-benzene). Upon cooling the filtered reaction solution to −30 °C, single crystals of $\mathbf{3_H}$/**4** suitable for SC-XRD were isolated in form of black needles in addition to free dppbz ligand and other unidentified and inseparable side-products. Reaction of the corresponding deuteride precursor, $[D_3Cu_3](dppz)_3$, leads to formation of $\mathbf{3_D}$ as clearly identified by *in situ* LIFDI-MS analysis (see Fig. S21, ESI†). Notably, from the related reaction of $[H_6Cu_6](PPh_3)_6$ with AlCp*, the smaller cluster $[H_4Cu_6Al_6](Cp^*)_6$ was isolated.[1] Obviously, reductive elimination of dihydrogen, H_2, leads to the formation of $[H_xCu_y]$ aggregates and the subsequent trapping by AlCp* yields $\mathbf{3_H}$/**4**. The influence of the phosphine (PPh_3 *vs.* dppbz) heteroatom ligand used on the $[Cu_aAl_b]$ cluster size is however unclear so far and will be subject of further research.

Size focusing to the cluster composite $\mathbf{3_H}$/4 and selective synthesis of cluster 4. Size-focusing of the mixture of the discussed interrelated Cu/Al clusters in favor of the cluster pair $[Cu_7Al_6](Cp^*)_6$ (**3**) and $[Cu_8Al_6](Cp^*)_6$ (**4**) was possible by starting from AlCp* and CuMes (molar ratio 1 : 0.28) at 75 °C, followed after 4 h by addition of another 0.54 eq. of CuMes and further heating to 75 °C for 18 h (Scheme 2; overall Cu : Al stoichiometry applied 1 : 1.22). If the reaction of the organometallic sources of Cu and Al is conducted in precisely this way, the product clusters **3** and **4** are the major components in the equilibrated reaction mixture then observed in LIFDI-MS analysis (Fig. S18, ESI†). The reaction is accompanied by formation of Mes_2AlCp^* and $AlMes_3$ as identified by *in situ* ^{1}H-NMR (Fig. S5†). Notably, compounds **1** and **2** are observed as transient intermediates in the reaction by ^{1}H-NMR analysis before and after addition of the second portion of CuMes, respectively. This underlines their role as building blocks in cluster growth reactions. From these reaction solutions, **3**/**4** can be obtained as micro-crystalline precipitate after cooling to −30 °C and washing with cold *n*-hexane in 25% isolated yield. It is noted that the use of slightly less CuMes in this size focused synthesis of **3**/**4** did not significantly change the molar ratio of **3** : **4** according to NMR and LIFDI-MS analysis. In this experiment, however, a mixture of **3** and **4** together with the hydridic species $\mathbf{3_H}$ is then detected.

Based on these results a selective synthesis of **4** was developed by subjecting the primarily obtained cluster composite **3**/**4** to different stoichiometric amounts of CuMes. Reaction with 5 molar eq. of CuMes leads to a complete consumption of $[Cu_7Al_6](Cp)_6$ as identified by *in situ* LIFDI-MS as well as ^{1}H-NMR (vanishing of the corresponding paramagnetic signal even

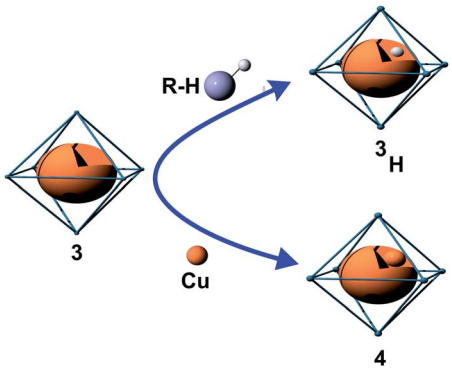

Scheme 3 Illustration of the reaction behavior of the radical species **3** $[Cu_7Al_6](Cp^*)_6$ towards R–H (R = toluyl, silyl) and towards Cu sources. See also Fig. 6 and the text for a rationalization of the radical reactivity of **3** in terms of molecular orbitals.

after short reaction times at room-temperature, see Fig. S6 and S19†). Again, the reaction is accompanied by formation of Mes_2AlCp^* and $AlMes_3$. Quantitative analysis of the ^{1}H-NMR spectra indicates increasing quantities of **4** being fully consistent with the LIFDI-MS spectra showing **4** as the only intense signal after 5 h reaction time. Indeed, single crystals of **4** were obtained from the filtered reaction solution in very small yield upon cooling to −30 °C. TEM images of evaporated reaction solutions again show the presence of smaller (5 nm) and larger Cu nano particles (*ca.* 50 nm) (see Fig. S34†). It can be assumed that due to its open-shell character, **3** is more reactive towards and is thus converted to **4**, while **4** remains initially unreacted (see Scheme 3 for illustration). However, both clusters **3** and **4** are expected to be susceptible to cluster growth reactions with CuMes and this may lead to larger clusters in the reaction solution which cannot any more be observed by our LIFDI-MS instrumentation at this point of methodological development.

Characterization of isolated species

Crystallographic results. Crystals suitable for SC-XRD of **1**, **2**, $\mathbf{3_H}$/**4** and **4** were obtained by cooling of the respective, filtered reaction solutions to −30 °C for several days. Fig. 2 displays the refined molecular structures. For a detailed crystallographic discussion, we refer to the ESI (Fig. S30–S32†). The $[Cu_2Al](Cp^*)_3$ cluster **2** is isostructural and isoelectronic to $[CuZn_2](Cp^*)_3$ (see Fig. 2).[34] The Cu/Al distribution in **2** is disordered over all three positions. Thus, all structural parameters involving the metal core are less precise and will therefore be discussed only on a qualitative level.

1 consists of a Cu_4Al trigonal bipyramid, (Cu_1–Cu_4, Al_1), whereby the central Cu_2 unit is additionally coordinated by two "terminal" (Al_2, Al_4) as well as one bridging (Al_3) AlCp* ligand. Interestingly, to the best of our knowledge, **1** is the first crystallographically characterized compound featuring an Al^IMes ligand. Alternatively, a Cu_4 butterfly structural motif can be distinguished in the structure of **1**, which is known from other molecular Cu clusters like $[Cu_4Te_4](PiPr)_4$ (ref. 45) and $[Cu_4](PPh_3)_2(mt)_4$ (ref. 46) (mt = 2-mercaptothiazoline). Interestingly, similar structural motifs can also be identified in larger Cu/Al clusters. In this context, the structure of $\mathbf{3_H}$/**4** can be described as a superposition of two AlCp* capped Cu-butterfly

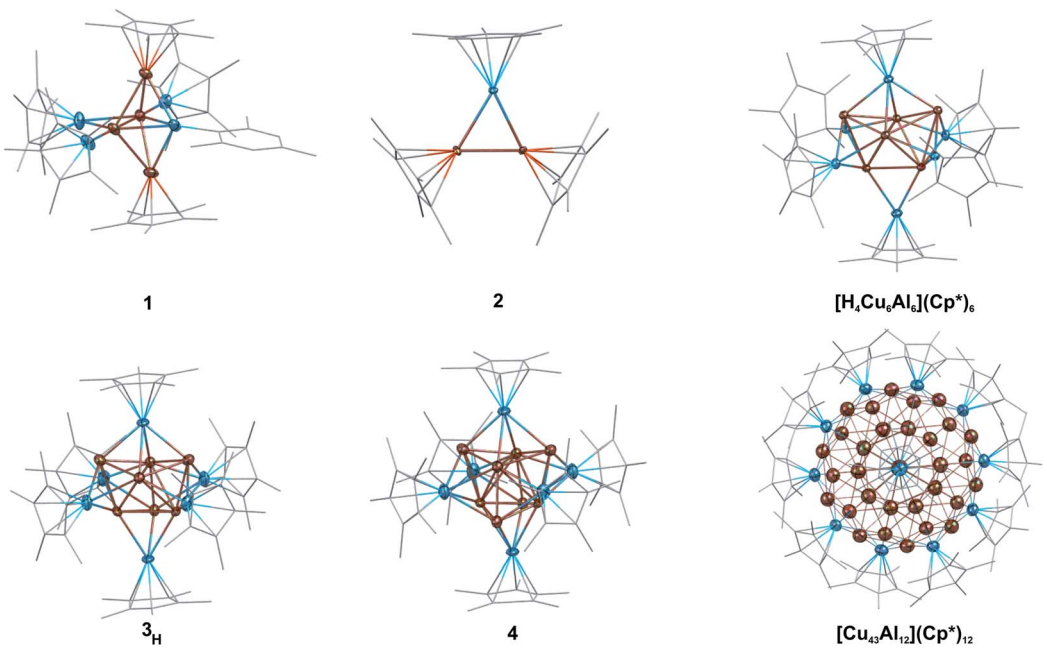

Fig. 2 Representation of the molecular structures of the new, fully characterized clusters **1**, **2**, $\mathbf{3_H}$ and **4**, as well as of the previously reported clusters $[H_4Cu_6Al_6](Cp^*)_6$ (ref. 1) and $[Cu_{43}Al_{12}](Cp^*)_{12}$.[2] Color code: Cu = dark orange, Al = blue. The molecular structures in the solid state were obtained by SC-XRD. Thermal ellipsoids are shown at the 50% probability level, hydrogen atoms, co-crystallized solvent molecules and disordered groups are omitted for clarity and ligands are simplified as wireframes. Full details of the structure determination are given in the ESI.†

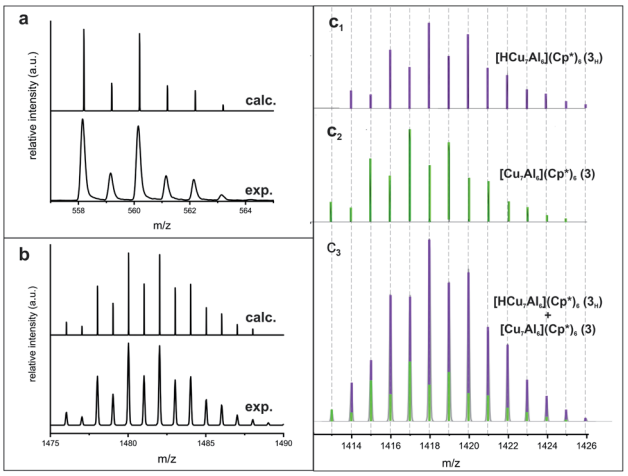

Fig. 3 (a) Comparison of calculated (top) and experimental (bottom) isotopic patterns of **2** as determined by LIFDI-MS. (b) Comparison of calculated (top) and experimental (bottom) isotopic patterns of **4** as determined by LIFDI-MS. (c_1/c_2) Visualization of the hydride shift of one *m*/*z* unit by comparison of calculated mass spectra of **3** and $\mathbf{3_H}$ (see Fig. S21† for experimental mass envelopes). (c_3) Isotopic pattern (experimental, determined by LIFDI-MS) of a mixture of **3**/$\mathbf{3_H}$ as determined by LIFDI-MS after heating of **3** in toluene (110 °C, 5 days). Fractions of **3** and $\mathbf{3_H}$ are illustrated in green and purple, respectively.

motifs (see Fig. 4a). An Al atom surrounded by four butterfly-like arranged Cu atoms is also found in the molecular structure of $[H_4Cu_6Al_6](Cp^*)_6$,[1] while in $[Cu_{43}Al_{12}](Cp^*)_{12}$, AlCp* occupies positions capping Cu_3 triangular faces.[2] In view of these structural analogies, **1** can be seen as a native "building block" for larger Cu/Al aggregates.

Likewise, the embryonic character of **2** is reflected in the appearance of its almost equilateral triangular Cu_2Al motif in **1**, whereas in larger clusters a direct comparison is difficult due to the lack of CuCp* moieties. In general, the structure of $\mathbf{3_H}$/**4** compromises a core of two nested copper tetrahedra embedded into an AlCp* octahedron. Hereby, the outermost Cu positions are only partially occupied (composition according to refined crystal structure: $[Cu_{7.33}Al_6](Cp^*)_6$), being well consistent with a composite of $[HCu_7Al_6](Cp^*)_6$ and $[Cu_8Al_6](Cp^*)_6$ as determined by LIFDI-MS (*vide supra*).

In general, the structure of $\mathbf{3_H}$/**4** compromises a core of two nested copper tetrahedra embedded into an AlCp* octahedron. Hereby, the outermost Cu positions are only partially occupied composition according to refined crystal structure: $[Cu_{7.33}Al_6](Cp^*)_6$, being well consistent with a composite of $[HCu_7Al_6](Cp^*)_6$ and $[Cu_8Al_6](Cp^*)_6$ as determined by LIFDI-MS (*vide supra*).

The hydride could not be located by SC-XRD but DFT calculations allow for an assessment of its binding mode (*vide infra*). Contrary and as expected, the structure of **4** (SC-XRD data of the isolated pure compound) compromises a fully occupied $[Cu_8]$ kernel. The faces of the inner Cu tetrahedron are capped by the Cu atoms of the outer Cu tetrahedron resulting in an overall structural motif, which is well known as "stella quadrangula" from corresponding Hume-Rothery phases like γ-brass (Cu_5Zn_8) or Cu_9Al_4.[47] We would like to emphasize the structural relationship between the species $[H_4Cu_6Al_6](Cp^*)_6$ (dicapped tetrahedron)[1] $[Cu_7Al_6](Cp^*)_6$ (triple capped tetrahedron) and $[Cu_8Al_6](Cp^*)_6$ (tetracapped tetrahedron) (see Fig. 4b). Additionally, the tetracapped tetrahedron to tricapped tetrahedron relationship is documented in the literature for homometallic copper clusters, although featuring not Cu(0) but Cu(I).[48,49]

Triangular motifs are common in all three compounds. Whereas **2** itself is an almost equilateral triangle, in **1**, the central triangle of the bipyramid exhibits an angle of 57.75(3)°. The triangular faces of the inner tetrahedron in $\mathbf{3_H}$/**4** span almost equilateral triangles with bond angles close to 60°. The outer tetrahedron itself is spanned by almost equilateral triangles.

Analytical and spectroscopic characterization. Composition and identity of compounds **1** and **2** and of the composite **3**/**4** were confirmed by full characterization ($^1H/^{13}C$-NMR, LIFDI-MS, elemental analysis, ATR-IR) and the results are presented in the ESI.† It is noted that despite lack of SC-XRD analysis of **3**/**4** (poor crystal quality), it can be regarded as isostructural to the closely related composite $\mathbf{3_H}$/**4** according to powder-Xray diffraction analysis (see ESI, Fig. S27†). For composite $\mathbf{3_H}$/**4** no elemental/NMR/IR analysis is possible as it crystallizes as an inseparable mixture with free dppbz ligand and unidentified, hydride containing side-products. All attempts of isolating the single crystals under an optical microscope for further analysis were unsuccessful. However, the presence of the hydride in $\mathbf{3_H}$ is unequivocally indicated by LIFDI-MS analysis and isotopic labeling experiments starting from the corresponding Cu(I)-deuteride precursor (see ESI, Fig. S21†). This highlights the strength of mass-spectrometry and labeling studies for analysis of subtle differences between cluster species even in mixtures.

Elemental analysis of micro-crystalline **3**/**4** closely matches the values expected for $[Cu_8Al_6](Cp^*)_6$ indicating that the amount of $[Cu_7Al_6](Cp^*)_6$ is below 5 mass%. This is in full agreement with SQUID measurements of the sample, indicating an overall diamagnetic behavior over the whole temperature range with only very small paramagnetic contributions.

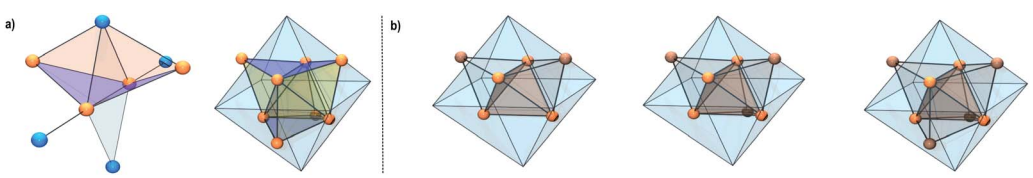

Fig. 4 (a) Illustration of the butterfly $[Cu_4]$ motif in **1** (left) and **4** (right). (b) Structural evolution of the Cu-kernels in $[H_4Cu_6Al_6](Cp^*)_6$, $\mathbf{3_H}$ and **4** (from left to right).

Electronic structure characterization

A rationalization of the bonding in **1** can start in considering it as made of six building units, namely one (edge-bridging) Al(η^5-Cp*), one Al-Mes, two Cu(η^5-Cp*) and two "linear" Cu–Al(η^5-Cp*) fragments. Assuming that six electrons are used for Cp* to M bonding (M = Al, Cu) and that the Cu–Al terminal bonds are localized 2-electron bonds, then the Al(η^5-Cp*), Al-Mes, Cu(η^5-Cp*) and "linear" Cu–Al(η^5-Cp*) fragments are 2-, 2-, 0- and 1-electron donors, respectively. Therefore, one is left with 6 electrons for the bonding within the $[Cu_4Al_2]$ inner core of **1**. The M(η^5-Cp*) (M = Al, Cu) fragments have only one σ-type hybrid orbital to participate to the bonding. The Cu–R (R = AlCp*) and Al–R (R = Mes) units have three orbitals available. One is a σ-type hybrid and two are π-type np AOs, *i.e.*, "perpendicular" to the M–R bond.[50] With such a fragment orbital manifold and looking at the $[Cu_4Al_2]$ core as an edge-bridged $[Cu_4Al]$ trigonal bipyramid, it is easy to predict that there are only two bonding combinations of the fragment frontier orbitals that can be associated with the $[Cu_4Al]$ trigonal bipyramid. They are the in-phase combination of the five σ-type hybrid and the π-bonding combination on the $[Cu_2Al]$ triangular base of the bipyramid, stabilized by the out-of-phase combination of the two σ-type hybrids of the CuCp* capping units. These orbitals are sketched in Scheme S5† (left side and middle). They contain four of the six cluster electrons. The remaining electron pair is associated with the 2-electron/3-center bonding between the μ_2-AlCp* fragment and the Cu–Cu edge it bridges (right side of Scheme S5†). Indeed the "linear" Cu-AlCp* units have enough frontier orbitals to participate to three bonding pairs.

This qualitative picture is supported by DFT calculations on **1** and on a simplified and symmetrized model of **1** in which all the methyl groups were replaced by hydrogens (see Fig. 6a). In the real cluster **1** the two "σ-type" cluster MOs of Scheme S5† somehow mix together and some supplementary mixing also occurs with other cluster MOs, in particular with those associated with the terminal Al–Cu bonds. The major computed data for **1** are gathered in Table S6.† There is a good agreement between the optimized geometry and the X-ray structure. The computed ^{1}H- and ^{13}C-NMR chemical shifts match also nicely with their experimental counterparts (Fig. S37 and S38†). From the Wiberg bond indices (WBI) one can see that the strongest Al–Cu bonds are those between Al(Mes) and the two Cu(Cp*) atoms. Cu–Cu bonding appears relatively weak (WBI_{av} = 0.065). As expected, the more positively charged Cu and Al atoms are those bonded to Cp* ligands. It is of note that the Cp* ligands play a crucial role in stabilizing the structure of the very electron-deficient cluster **1**. Indeed, when the Cp*s are replaced by simple Cps in the calculation, the structure collapses during the geometry optimization process. The effect of the Cp* ligands is of double nature: their electron-donating ability tends to satisfy as best as possible the electron demand of the cluster core, and they constitute a tight and rather rigid protecting shell around the cluster. Such a shield effect of Cp* ligands around metal cluster cores is already well documented.[1,2,18,30]

The DFT-optimized structure of **2** is of approximate C_{2v} symmetry, with Cu–Al bonds of 2.294 and 2.295 Å and a Cu–Cu bond of 2.421 Å. These values are expected to be more accurate than their X-ray counterparts (see above). The corresponding WBI values are 0.559, 0.557 and 0.199, respectively. Cu–Cu bonding in **2** is thus much stronger than in **1**. The 3-center/2-electron bonding within the triangle is made of the in-phase combination of the unique σ-type hybrid frontier orbital of the three MCp* (M = Cu, Al) constituting fragments and the two electrons provided by the AlCp* units. The corresponding Kohn–Sham orbital is the HOMO−7. It is plotted in Fig. 6b. Thus, **2** is isoelectronic to $[Zn_2Cu](Cp^*)_3$,[34] or more simply, $[H_3]^+$. For the sake of comparison, the optimized geometry of the isoelectronic homometallic $\{[Cu_3](Cp^*)_3\}^{2-}$ hypothetical anion yielded Cu–Cu distances and WBI of 2.389 Å and 0.412, respectively, *i.e.* stronger Cu–Cu bonding than in **2**. The ^{1}H- (2.0 and 1.7 ppm) and ^{13}C-NMR chemical shift (Fig. S37†) computed for **2** are in good agreement with their experimental counterparts.

The rather compact $Cu_4@Cu_4@Al_6$ shell arrangement of the inner core in **4** suggests looking at it as a superatom[51–56] with an electronic structure that can be rationalized within the spherical jellium model.[57] Indeed, its number of core bonding electrons (1 × 8 (Cu) + 2 × 6 (AlCp*) = 20) is one of the closed-shell stability "magic" numbers predicted by this model. It corresponds to the $1S^2\ 1P^6\ 1D^{10}\ 2S^2$ jellium electron configuration (the 3d(Cu) electrons are not supposed to be involved in this count[2]). This is confirmed by our DFT calculations on **4** and on a simplified model in which the Cp* ligands were replaced by Cps. In the latter model, ten occupied Kohn–Sham orbitals can be easily identified as the jellium orbitals containing the 20 cluster electrons (Fig. S38†). They clearly derive from the jellium orbitals of the bare $[Cu_8Al_6]^{6+}$ core, as illustrated in Fig. S39,† and are only weakly perturbed by the passivating ligand shell.[58] The computed HOMO–LUMO gap of **4** is 1.17 eV and the HOMO, which is the weakly bonding 2S orbital (Fig. 6c, left side), lies 0.90 eV above the HOMO−1, which is of 1D nature. This situation suggests that **4** could be easily oxidized, generating a 19-, perhaps 18-electron, species. Relevant computed data are given in Table S7.† The Wiberg indices are consistent with weak and strong Cu–Cu (WBI_{av} = 0.025) and Al–Cu (WBI_{av} = 0.289) bonding, respectively. As for **1** and **2**, the computed ^{1}H- (1.8 ppm) and ^{13}C-NMR (115.2 and 12.9 ppm) chemical shifts are in line with their experimental counterparts (*vide supra*). Removing one of the Cu_2/Cu_{2a} second-shell atoms in **4** (see Fig. 2 and 4b), generates the $[Cu_4@Cu_3@Al_6](Cp^*)_6$ odd-electron cluster **3**, with limited structural changes (see Table S7†) of the optimized geometry and a still rather spherical molecular shape. From the electronic structure point of view, when going from **4** to **3**, one loses one 4s(Cu) orbital (involved in cluster bonding) and the electron it contains. The result is a limited weakening of the bonding character in the occupied jellium orbitals. On the other hand, the electron loss generates a paramagnetic 19-electron superatom, with a singly occupied 2S HOMO (Fig. 6c, right side). This situation is somewhat related to that of the 19-electron gas-phase $[Cu_{18}]^-$ cluster.[59] This SOMO resembles somewhat the HOMO of **4** but is

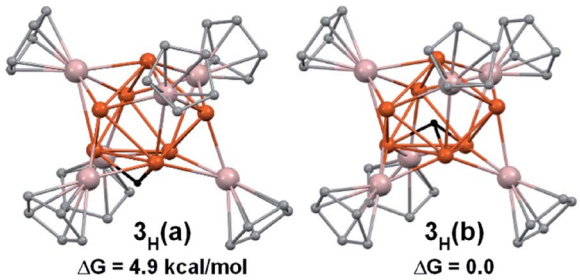

Fig. 5 The two computed isomers of 3_H and their relative free enthalpies *G* (methyl groups omitted for clarity). The μ_3-hydride is shown in black.

polarized on the capping Cu atom *trans* to its "missing" congener. It also gets some contribution from three Al atoms (Fig. 6c and Table S7†). The computed value of the ^{1}H-NMR chemical shifts of **3** (1.9 and 1.7 ppm) match approximately with the observed paramagnetic signal of −1.03 ppm. The hypothetical 20-electron anion 3^- adopts a rather similar structure with a substantial HOMO–LUMO gap of 1.23 eV. Going from **3** to 3_H also restores the closed-shell "magic" 20-electron configuration and provides an additional 1s(H) orbital that can participate to cluster bonding. Two low-energy isomers were found (Fig. 5 and Table S7†). In 3_H**(a)** the hydride occupies the μ_3 capping position of the "missing" copper atom in **3**, In the isomer 3_H**(b)**, which is the most stable by 5 kcal/mol^{-1}, the hydride sits inside the copper cage (H@Cu_4@Cu_3@Al_6). Owing to the elongated shape of the inner Cu_4 tetrahedron, the hydride does not occupy its very center, but lies close to the smaller Cu_3 triangular face, in a μ_3 bonding mode. This configuration exhibits a large HOMO–LUMO gap of 1.81 eV. It is of note that, in both 3_H**(a)** and 3_H**(b)** isomers, the hydride caps the same Cu_3 face, but in an outer and inner position, respectively. In both isomers, the hydride NAO charge is substantially negative (−0.35 and −0.58, respectively). The corresponding computed ^{1}H-NMR chemical shifts are also negative (−21.8 and −52.4 ppm, respectively). Test calculations indicate that these extremely shielded values remain stable upon functional and basis set changes. One should also note that all the other ^{1}H-NMR chemical shifts computed for compounds **1–4** agree with their experimentally recorded counterparts (see above and Fig. S37–S39†) and that values of the order of −50 ppm are known.[60] In any case, the hydride in 3_H**(b)** (or 3_H**(a)**), is likely to be fluxional, rendering its NMR signal detection problematic.

C–H and Si–H activation

When isolated **3**/**4** is heated in toluene to 110 °C for several days, LIFDI-MS analysis of the solution indicated partial transformation of **3** into 3_H (see Fig. $3c_3$ and Scheme 3). Pentamethylfulvene was identified as an organic reaction product by GC-MS (see Table S5†). However, no reaction at all is observed in toluene-d_8 (also no formation of pentamethylfulvene according to ^{1}H-NMR analysis) indicating C–H bond activation of toluene playing a crucial role in the reaction pathway. We suggest a mechanism, in which **3** initially reacts with toluene by H radical transfer forming 3_H and toluyl radicals, which intermolecularly C–H activate Cp* ligands in a second reaction step, finally resulting in formation of pentamethylfulvene. The presence of the "deprotected" cluster $[Cu_8Al_6](Cp^*)_5$ as a small peak in LIFDI-MS analysis is consistent with this hypothesis (see Fig. S23, ESI†). It is noted that substantial isotope effects in such H atom transfer reactions from toluene are known in literature.[61]

The reactive open-shell character of **3** is further illustrated by conversion of isolated **3**/**4** with TTMS (tris(trimethylsilyl)silane) at 110 °C in toluene to a mixture of **3**/3_H/**4** in addition to $\{[Cu_7Al_6](Cp^*)_6(Si(SiMe_3)_3) - H\}$ and $\{[Cu_8Al_6](Cp^*)_6(Si(SiMe_3)_3) - H\}$ (see Fig. S24† and Scheme 3). *In situ* ^{1}H-NMR analysis indicates consumption of **3** (see Fig. S13†). Unfortunately, no signal of the hydride species 3_H could be observed, probably due the fluctional character of the hydride. *In situ* ^{1}H-NMR and GC-MS analysis of the reaction mixture reveals formation of a variety of polysilanes, such

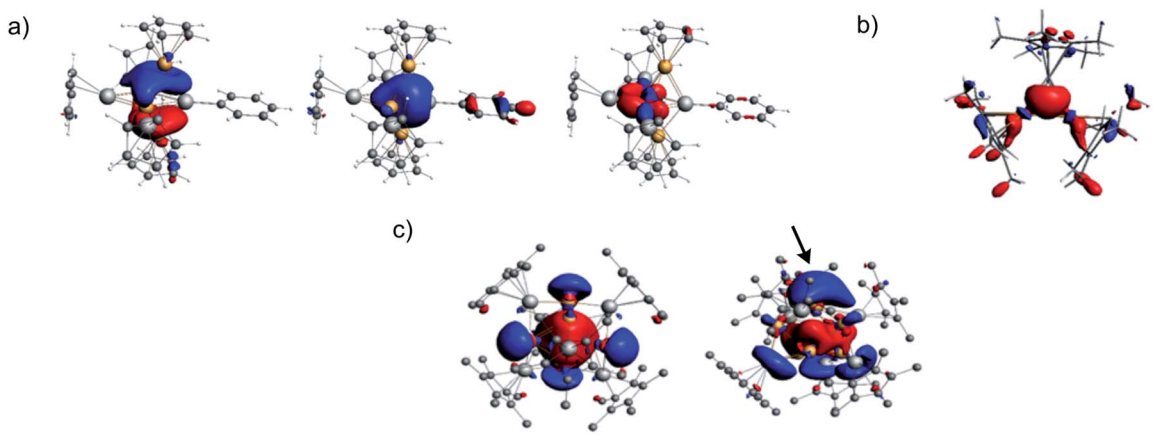

Fig. 6 (a) The three occupied Kohn–Sham orbitals containing the six metal–metal bonding electrons in the simplified model for **1**, $[Cu_4Al_4](Cp)_5(C_5H_5)$ (single-point calculation on a symmetrized model of C_s symmetry). (b) The 3-center bonding Kohn–Sham orbital (HOMO−7) associated with the 2-electron/3-center metal–metal bonding in **2**. (c) The HOMO of **4** (left) and SOMO of **3** (right). Polarization of the SOMO is marked by an arrow and is attributed to the radical reactivity of **3**.

as *e.g.* hexamethyldisilane, pentamethyldisilane or tetramethyldisilane (see Table S5†), pointing to a radical H-transfer mechanism. When **3**/**4** is converted with the deuterated analogon $(TMS)_3SiD$, a mixture of **3**/$\mathbf{3_H}$/$\mathbf{3_D}$/**4** is observed (see Fig. S26†). Reaction with tetrakis(trimethylsilyl)silane $(TMS)_4Si$ yielded a mixture of $\mathbf{3_H}$/**3** together with $\{[Cu_8Al_6](Cp^*)_6(SiMe_3) - H\}$ as novel species observed in LIFDI-MS analysis (see Fig. S27 and S28†). In this case, $(TMS)_3SiH$ together with pentamethylfulvene were detected in GC-MS analysis again pointing towards a radical H-transfer mechanism.

From these results we conclude that the reactive open shell cluster **3** is inclined to C–H and Si–H bond activation reactions with the corresponding closed shell hydride cluster $\mathbf{3_H}$ as the thermodynamically stable reaction product. While no C–D activation occurs with toluene-d_8 under the conditions applied, Si–D activation is observed, competitively occurring to the C–H activation reactions of toluene and of Si–CH_3 groups.

Summary and perspectives

Cluster growth reactions of intermetallic Cu/Al clusters were investigated by means of *in situ* LIFDI-MS and ^{1}H-NMR spectroscopy. Using this approach, we successfully isolated the thermally labile cluster $[Cu_4Al_4](Cp^*)_5(Mes)$ (**1**) as an early intermediate in the reaction between CuMes and AlCp*. Cluster **1** features the first example of a AlMes fragment, formally Al(I), which is part of a $[Cu_4Al]$ trigonal bipyramid. Targeted cluster degradation of **1** with excess of 3-hexyne allows isolation of the triangular, 2-electron cluster $[Cu_2Al](Cp^*)_3$ (**2**), the smallest possible member of the Cu/Al cluster family. Cluster growth reactions induced thermally or by specific addition of growth components involving isolated **1** and **2** were investigated by detailed variation of reaction parameters. We thereby discovered the inseparable cluster composite **3**/$\mathbf{3_H}$/**4**, which is a mixture of the paramagnetic, open shell superatomic cluster $[Cu_7Al_6](Cp^*)_6$ (**3**) and its closed shell hydride congener $[HCu_7Al_6](Cp^*)_6$ ($\mathbf{3_H}$) as well as the closed-shell cluster $[Cu_8Al_6](Cp^*)_6$ (**4**), which contains just one Cu core atom more than cluster **3**. Only the radical species **3** was shown to be reactive towards C–H and Si–H activation reactions of toluene and $(TMS)_3SiH$, respectively. The stability and low reactivity of the $\mathbf{3_H}$ and **4** clusters is in line with their magic 20-electron superatomic counts, although not all superatoms with magic counts are inert. While our results help to understand a variety of chemical processes in the early stage of intermetallic Cu/Al cluster formation, the present study certainly also transcends these immediate outcomes by presenting a methodological approach for the elucidation of reactivity patterns in complex cluster mixtures. Based on LIFDI mass spectrometry and different spectroscopic techniques, the analysis of reaction events in cluster mixtures is rendered possible and efficient without the need to isolate singular clusters. Further work in our group will focus on the selective generation and deeper understanding of larger and more diverse Cu/Al cluster libraries (see Fig. S40† for illustration). Our cluster repertoire in this and previous studies includes mostly small to medium sized TM/E clusters (TM = transition metal, *E* = group 12/13 metal) with structural frameworks similar to Fig. S40a or b.† Both cluster types are based on a core/shell structure with either the TM (Fig. S42a†)[12,13] or the main group metal *E* (Fig. S40b†)[40,41] in the inner core. We could demonstrate on various examples, that the organic protective ligand layer (as represented by the semi-transparent grey shell in Fig. S40†) is in principle either penetrable or partially removable by *e.g.* hydrogenolysis, protolysis or selective one electron oxidation reactions,[7] allowing reactivity studies of such clusters with small organic molecules.[13] We also succeeded in the isolation and characterization of the large intermetallic cluster $[Cu_{43}Al_{12}](Cp^*)_{12}$ (ref. 12) with fully ligand protected core/shell type structure as shown in S40c.† However, penetration of the organic ligand shell proved unsuccessful in this example so far, which is basically a consequence of the complete insolubility of this compound. Our long-term strategic goal, however, is the generation of large intermetalloid clusters with random element distribution and open coordination sites (Fig. S40d†) which we hope to set in use for model studies of structure/reactivity relationships in intermetallic materials. We suggest that the basic strategy presented in this work, *i.e.* the generation as well as reactivity testing of intermetalloid cluster libraries is a promising approach towards this goal. For example, a large cluster library (>10 species) with reproducible composition is observed in reaction solutions obtained from the minimalistic building block $[Cu_2Al](Cp^*)_3$ (**2**) and $[H_6Cu_6](L)_6$ (L = PPh_3). We intend to explore these clusters and their reactivity as a function of electronic structure, and we will report on our findings in future publications.

Author contributions

Max Schütz: experimental work, single crystal X-ray data acquisition and analysis, manuscript preparation; Christian Gemel: (computerized) data interpretation, manuscript preparation; Maximilian Muhr: initial DFT calculations; Christian Jandl: single crystal data acquisition and analysis; Samia Kahlal: DFT calculations and theoretical bonding analysis; Jean-Yves Saillard: DFT calculations, theoretical bonding analysis and manuscript preparation; Roland A. Fischer: research conception, manuscript preparation.

Conflicts of interest

There are no conflicts to declare.

Acknowledgements

This work was funded by the German Research Foundation (DFG) within a Reinhard Koselleck Project (FI-502/44-1). Prof. T. Fässler (TUM) and Prof. O. Cador (Univ. Rennes) are acknowledged for help with SQUID data acquisition and analysis. Tomanec Ondřej and Prof. Radek Zboril (Regional Center of Advanced Technologies and Materials, 78371 Olomouc, Czech Republic) are acknowledged for their valuable help with HRTEM measurements and EDX data analysis of Cu nanoparticles. Prof. Inoue (TUM) is acknowledged for grateful donation of $(TMS)_3SiBr$. Richard Weininger and Matthias Huber are acknowledged for their help in organometallic

precursor synthesis and the conduction of LIFDI-MS measurements. We are grateful to the GENCI (Grand Equipement National de Calcul Intensif) for HPC resources (Project A0050807367).

References

1 C. Ganesamoorthy, J. Weßing, C. Kroll, R. W. Seidel, C. Gemel and R. A. Fischer, *Angew. Chem., Int. Ed.*, 2014, **53**, 7943–7947.

2 J. Weßing, C. Ganesamoorthy, S. Kahlal, R. Marchal, C. Gemel, O. Cador, A. C. Da Silva, J. L. Da Silva, J. Y. Saillard and R. A. Fischer, *Angew. Chem., Int. Ed.*, 2018, **57**, 14630–14634.

3 G. Schmid, R. Pfeil, R. Boese, F. Bandermann, S. Meyer, G. Calis and W. Vandervelden, *Chem. Ber./Recl.*, 1981, **114**, 3634–3642.

4 N. Jian, C. Stapelfeldt, K.-J. Hu, M. Fröba and R. E. Palmer, *Nanoscale*, 2015, **7**, 885–888.

5 V. K. Ocampo-Restrepo, L. Zibordi-Besse and J. L. Da Silva, *J. Chem. Phys.*, 2019, **151**, 214301.

6 S. Hirabayashi and M. Ichihashi, *J. Phys. Chem. A*, 2015, **119**, 8557–8564.

7 S. Furukawa and T. Komatsu, *ACS Catal.*, 2017, **7**, 735–765.

8 M. Guo, B. Yin, B. Huang, H. Wu and Z. Luo, *J. Mater. Chem. C*, 2020, **8**, 10325–10332.

9 S. M. Lang and T. M. Bernhardt, *Phys. Chem. Chem. Phys.*, 2012, **14**, 9255–9269.

10 U. Heiz, A. Sanchez, S. Abbet and W.-D. Schneider, *J. Am. Chem. Soc.*, 1999, **121**, 3214–3217.

11 A. Sanchez, S. Abbet, U. Heiz, W.-D. Schneider, H. Häkkinen, R. Barnett and U. Landman, *J. Phys. Chem. A*, 1999, **103**, 9573–9578.

12 W. Bouwen, P. Thoen, F. Vanhoutte, S. Bouckaert, F. Despa, H. Weidele, R. E. Silverans and P. Lievens, *Rev. Sci. Instrum.*, 2000, **71**, 54–58.

13 A. I. Ayesh, N. Qamhieh, S. T. Mahmoud and H. Alawadhi, *J. Mater. Res.*, 2012, **27**, 2441.

14 D. Cox, K. Reichmann, D. Trevor and A. Kaldor, *J. Chem. Phys.*, 1988, **88**, 111–119.

15 X.-N. Li, L.-N. Wang, L.-H. Mou and S.-G. He, *J. Phys. Chem. A*, 2019, **123**, 9257–9267.

16 X. P. Zou, L. N. Wang, X. N. Li, Q. Y. Liu, Y. X. Zhao, T. M. Ma and S. G. He, *Angew. Chem.*, 2018, **130**, 11155–11159.

17 R. A. Fischer and J. Weiß, *Angew. Chem., Int. Ed.*, 1999, **38**, 2830–2850.

18 S. Gonzalez-Gallardo, T. Bollermann, R. A. Fischer and R. Murugavel, *Chem. Rev.*, 2012, **112**, 3136–3170.

19 T. Bollermann, C. Gemel and R. A. Fischer, *Coord. Chem. Rev.*, 2012, **256**, 537–555.

20 K. Mayer, J. Weßing, T. F. Fässler and R. A. Fischer, *Angew. Chem., Int. Ed.*, 2018, **57**, 14372–14393.

21 L. Xu and S. C. Sevov, *Inorg. Chem.*, 2000, **39**, 5383–5389.

22 S. Mitzinger, L. Broeckaert, W. Massa, F. Weigend and S. Dehnen, *Nat. Commun.*, 2016, **7**, 1–10.

23 R. J. Wilson, N. Lichtenberger, B. Weinert and S. Dehnen, *Chem. Rev.*, 2019, **119**, 8506–8554.

24 S. Scharfe, F. Kraus, S. Stegmaier, A. Schier and T. F. Faessler, *Angew. Chem., Int. Ed.*, 2011, **50**, 3630–3670.

25 J. Vollet, J. R. Hartig and H. Schnöckel, *Angew. Chem., Int. Ed.*, 2004, **43**, 3186–3189.

26 S. K. Barik, S.-C. Huo, C.-Y. Wu, T.-H. Chiu, J.-H. Liao, X. Wang, S. Kahlal, J.-Y. Saillard and C.-W. Liu, *Chem.–Eur. J.*, 2020, **26**, 10471–10479.

27 T. Steinke, C. Gemel, M. Winter and R. A. Fischer, *Angew. Chem., Int. Ed.*, 2002, **41**, 4761–4763.

28 B. Buchin, T. Steinke, C. Gemel, T. Cadenbach and R. A. Fischer, *Z. Anorg. Allg. Chem.*, 2005, **631**, 2756–2762.

29 K. Freitag, H. Banh, C. Gemel, R. W. Seidel, S. Kahlal, J.-Y. Saillard and R. A. Fischer, *Chem. Commun.*, 2014, **50**, 8681–8684.

30 H. Banh, J. Hornung, T. Kratz, C. Gemel, A. Pöthig, F. Gam, S. Kahlal, J.-Y. Saillard and R. A. Fischer, *Chem. Sci.*, 2018, **9**, 8906–8913.

31 M. Schütz, M. Muhr, K. Freitag, C. Gemel, S. Kahlal, J.-Y. Saillard, A. C. Da Silva, J. L. Da Silva, T. F. Fässler and R. A. Fischer, *Inorg. Chem.*, 2020, **59**, 9077–9085.

32 C. Gemel, T. Steinke, D. Weiss, M. Cokoja, M. Winter and R. A. Fischer, *Organometallics*, 2003, **22**, 2705–2710.

33 A. Schnepf and H. Schnöckel, *Angew. Chem., Int. Ed.*, 2002, **41**, 3532–3554.

34 K. Freitag, C. Gemel, P. Jerabek, I. M. Oppel, R. W. Seidel, G. Frenking, H. Banh, K. Dilchert and R. A. Fischer, *Angew. Chem., Int. Ed.*, 2015, **54**, 4370–4374.

35 P. J. Dyson, B. F. Johnson, J. S. McIndoe and P. R. Langridge-Smith, *Rapid Commun. Mass Spectrom.*, 2000, **14**, 311–313.

36 P. J. Dyson, A. K. Hearley, B. F. Johnson, T. Khimyak, J. S. McIndoe and P. R. Langridge-Smith, *Organometallics*, 2001, **20**, 3970–3974.

37 C. P. Butcher, A. Dinca, P. J. Dyson, B. F. Johnson, P. R. Langridge-Smith and J. S. McIndoe, *Angew. Chem., Int. Ed.*, 2003, **42**, 5752–5755.

38 C. P. Butcher, P. J. Dyson, B. F. Johnson, T. Khimyak and J. S. McIndoe, *Chem.–Eur. J.*, 2003, **9**, 944–950.

39 C. Evans, K. M. Mackay and B. K. Nicholson, *J. Chem. Soc., Dalton Trans.*, 2001, 1645–1649.

40 M. Muhr, P. Heiß, M. Schütz, R. Bühler, C. Gemel, M. H. Linden, H. B. Linden and R. A. Fischer, *Dalton Trans.*, to be submitted.

41 R. Benn, E. Janssen, H. Lehmkuhl and A. Rufínska, *J. Organomet. Chem.*, 1987, **333**, 155–168.

42 D. L. Reger and M. F. Huff, *Organometallics*, 1990, **9**, 2807–2810.

43 D. W. Macomber and M. D. Rausch, *J. Am. Chem. Soc.*, 1983, **105**, 5325–5329.

44 R. Drescher, S. Lin, A. Hofmann, C. Lenczyk, S. Kachel, I. Krummenacher, Z. Lin and H. Braunschweig, *Chem. Sci.*, 2020, **11**, 5559–5564.

45 D. Fenske and J. C. Steck, *Angew. Chem., Int. Ed.*, 1993, **32**, 238–242.

46 J. P. Fackler, C. A. López, R. J. Staples, S. Wang, R. Winpenny and R. P. Lattimer, *J. Chem. Soc., Chem. Commun.*, 1992, 146–148.

47 H. Nyman and S. Andersson, *Acta Crystallogr., Sect. A: Cryst. Phys., Diffr., Theor. Gen. Crystallogr.*, 1979, **35**, 934–937.
48 C. Latouche, S. Kahlal, Y.-R. Lin, J.-H. Liao, E. Furet, C. Liu and J.-Y. Saillard, *Inorg. Chem.*, 2013, **52**, 13253–13262.
49 P.-K. Liao, C.-S. Fang, A. J. Edwards, S. Kahlal, J.-Y. Saillard and C. Liu, *Inorg. Chem.*, 2012, **51**, 6577–6591.
50 T. A. Albright, J. K. Burdett and M.-H. Whangbo, *Orbital interactions in chemistry*, John Wiley & Sons, 2013.
51 S. Khanna and P. Jena, *Phys. Rev. Lett.*, 1992, **69**, 1664.
52 S. Khanna and P. Jena, *Phys. Rev. B: Condens. Matter Mater. Phys.*, 1995, **51**, 13705.
53 M. Walter, J. Akola, O. Lopez-Acevedo, P. D. Jadzinsky, G. Calero, C. J. Ackerson, R. L. Whetten, H. Grönbeck and H. Häkkinen, *Proc. Natl. Acad. Sci. U. S. A.*, 2008, **105**, 9157–9162.
54 Z. Luo and A. W. Castleman, *Acc. Chem. Res.*, 2014, **47**, 2931–2940.
55 T. Tsukuda and H. Häkkinen, *Protected metal clusters: from fundamentals to applications*, Elsevier, 2015.
56 B. Yin and Z. Luo, *Coord. Chem. Rev.*, 2020, 213643.
57 W. Knight, K. Clemenger, W. A. de Heer, W. A. Saunders, M. Chou and M. L. Cohen, *Phys. Rev. Lett.*, 1984, **52**, 2141.
58 Z. Luo, A. C. Reber, M. Jia, W. H. Blades, S. N. Khanna and A. Castleman, *Chem. Sci.*, 2016, **7**, 3067–3074.
59 B. Yin, Q. Du, L. Geng, H. Zhang, Z. Luo, S. Zhou and J. Zhao, *J. Phys. Chem. Lett.*, 2020, **11**, 5807–5814.
60 P. Garbacz, V. V. Terskikh, M. J. Ferguson, G. M. Bernard, M. Kedziorek and R. E. Wasylishen, *J. Phys. Chem. A*, 2014, **118**, 1203–1212.
61 K. A. Gardner and J. M. Mayer, *Science*, 1995, **269**, 1849–1851.